Low frequency sound attenuation in a flow duct using a thin slow sound material

Yves Aurégan[a)]
Laboratoire d'Acoustique de l'Université du Maine, Unite Mixte de Recherche 6613, Centre National de la Recherche Scientifique, Av. O Messiaen, F-72085 LE MANS Cedex 9, France
yves.auregan@univ-lemans.fr

Maaz Farooqui
Sound and Vibration Laboratory, Faculty of Engineering, Ain Shams University, 11517 Cairo, Egypt
maazfarooqui@gmail.com

Jean-Philippe Groby
Laboratoire d'Acoustique de l'Université du Maine, Unite Mixte de Recherche 6613, Centre National de la Recherche Scientifique, Av. O Messiaen, F-72085 LE MANS Cedex 9, France
Jean-Philippe.Groby@univ-lemans.fr

Abstract: A thin subwavelength material that can be flush mounted in a duct and that gives an attenuation band at low frequencies in air flow channels is presented. To decrease the material thickness, the sound is slowed in the material using folded side branch tubes. The impedance of the material is compared to the optimal value given by the Cremer condition, which can differ greatly from the air characteristic impedance. Grazing flow on this material increases the losses at the interface between the flow and the material.

[VEO]
Date Received: January 26, 2016 **Date Accepted:** April 19, 2016

1. Introduction

Ducts with airflow are used in many systems, such as ventilation in vehicles and buildings, gas turbine intake/exhaust systems, aircraft engines, see Fig. 1, etc. The associated generation of unsteady flow inevitably leads to noise problems. At low frequencies, this noise is very difficult to suppress or mitigate with devices having a thickness much smaller than the sound wavelength. There is a need for innovative acoustic materials efficient at low frequencies and able to cope with the stringent space constraints resulting from real applications.

To enhance the low frequency absorption, various solutions have been proposed like resonators embedded in porous materials or extended Helmholtz resonators (Li *et al.*, 2016). Recently the use of slow sound material has been proposed by Groby *et al.* (2015). By decreasing the effective compressibility in a tube (Aurégan and Pagneux, 2015), the effective sound velocity and, as a consequence, the material thickness can be drastically reduced.

The past researches on sound absorption with new materials were focused on absorbing panels or on the reflection at tube ends. Under normal incidence sound waves, the best attenuation is obtained when the acoustic impedance matches the air characteristic impedance $Z_0 = \rho_0 c_0$, where ρ_0 is the air density and c_0 is the sound velocity (hereinafter, all the impedances are normalized by Z_0). The situation is very different in ducts with airflow where the material is embedded in the wall, flush mounted to avoid any flow disturbance. The acoustic incident waves are no longer normal but tangential to the material. If the material is locally reacting (i.e., if the pressure and the normal velocity at the wall are linked by an impedance), the optimal impedance without flow at a frequency f for an infinitely long material is given by the Cremer optimal impedance (Tester, 1973a) by $Z_{\mathrm{Crem}} = (0.91 - 0.76\mathrm{i})\,2fH/c_0$ in a two-dimensional (2D) waveguide of height H. This impedance can differ significantly from the normal incidence one ($Z_{ni} = 1$) and the solutions developed in the latter case can be ineffective when the materials are flush-mounted in the wall of an airflow duct. Moreover, a mean flow is generally present in ducts and its effect on the acoustic

[a)]Author to whom correspondence should be addressed.

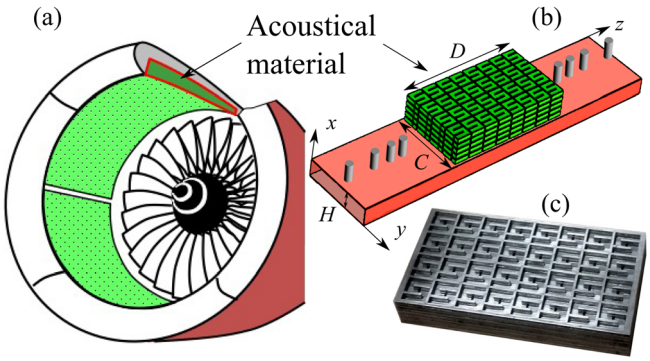

Fig. 1. (Color online) (a) Sketch of a turbofan engine intake where new thin materials acting at low frequencies are needed. (b) TSSM in a duct. (c) Picture of the manufactured TSSM where the first perforated plate is removed.

behavior of in-duct systems has to be studied. In this letter, we analyze the acoustic behavior of a thin slow sound material (TSSM) located on the sidewall of a rectangular duct without and with flow. This material has been optimized to provide a large attenuation in the low frequency range (around 600 Hz) despite of its small thickness (about 27 mm), which is significantly sub-wavelength. The thickness of a quarter wavelength resonator would be around 100 mm to be efficient in the same frequency range.

2. TSSM

The studied TSSM is composed of 4×8 identical cells. The dimension of each cell is $P \times P \times L_c$ with $P = 24$ mm and $L_c = 27$ mm [see Figs. 1(b) and 1(c) and Fig. 2]. The cell is composed of a central rectangular tube of size $A_c \times B_c \times L_c$ with $A_c = 2.2$ mm and $B_c = 6$ mm. One end of the central tube is connected to the airflow duct and the other is rigidly closed. On both large sides of the central tube, five side branches are connected, each of them is composed of folded rectangular tubes of size $A_s \times B_s \times L_s$ with $A_s = 4$ mm, $B_s = 6$ mm, and of neutral axis length $L_s = 34$ mm. The Γ-shape of the side tubes increases the compactness of the material and has an effect on the acoustic response: the effective length of those tubes, that has been computed using a finite element method (FEM) in 2D, is slightly changed in the frequency range of interest (see inset in Fig. 3). The entrance impedance of one cell has been measured with an impedance sensor (Le Roux *et al.*, 2012) and is displayed in thick black lines in Fig. 3.

The propagation in the folded side tubes can be derived from a wide tube approximation of the classical Kirchhoff's solution. The wavenumber is given by $k_s = k_0(1 + \Gamma_v + \Gamma_t)$, where Γ_v and Γ_t are complex numbers, respectively, related to viscous and thermal effects (Tijdeman, 1975). The normalized characteristic impedance of the side tube is $z_s = 1 + \Gamma_v - \Gamma_t$ and the entrance impedance of the folded side tubes is $Z_s = -\mathrm{i}z_s\cot(k_s L_s)$. In the low frequency limit ($k_s L_s \ll 1$), the side tubes impedance is given by $Z_s = -\mathrm{i}(1 - 2\Gamma_t)/(k_0 L_s)$, implying that the main dissipative effect is the thermal one at low frequencies.

In the central tube, two different models can be applied. The first one is a continuous model where the side loaded tubes are substituted by equivalent impedance applied on the sidewalls and the losses in the central tube are neglected. The propagation is governed by the Helmholtz equation: $\Delta p + k_0^2 p = 0$, where the pressure is sought in the form $p(x,y,f) = (c_1\sinh(\alpha y) + c_2\cosh(\alpha y))\exp(-\mathrm{i}k_c x)$, where $\alpha^2 = k_c^2 - k_0^2$. Here, x is the direction of the central tube axis and y is the transverse direction (see Fig. 4), the

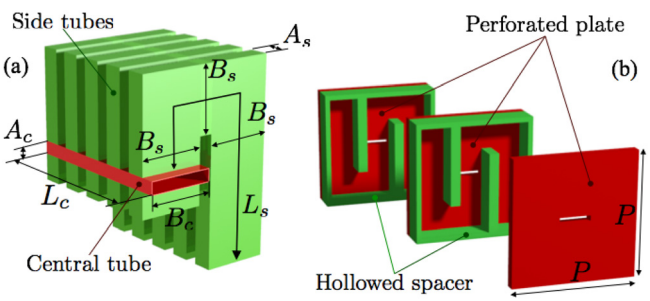

Fig. 2. (Color online) (a) Outline of the material where the bottom side tubes are cut for greater clarity. (b) Implementation of the TSSM with perforated plates and hollowed plates.

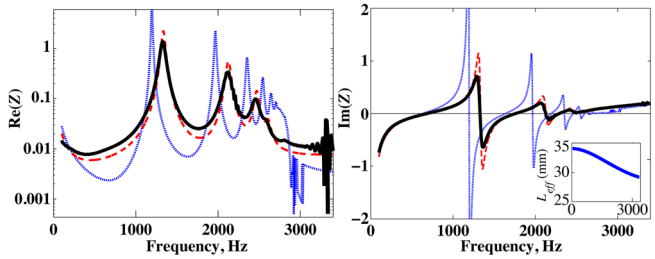

Fig. 3. (Color online) Real and imaginary part of the TSSM entrance impedance Z_c. The continuous black line is a direct measurement of the impedance of one cell, the dotted blue line is the impedance computed by the continuous model, and the dashed red line is the result of the lumped discrete model. The inset gives the effective length of the side tubes computed by FEM.

time convention $e^{i\omega t}$ is adopted where ω is the frequency and t is the time. The boundary condition for the wall located at $y=0$ is $p = iZ_s/(\Phi k_0)\partial_y p$, and for the wall at $y=A_c$ is $p = -iZ_s/(\Phi k_0)\partial_y p$, where Φ is the equivalent wall porosity. The propagation equation associated with the boundary conditions leads to the dispersion relation

$$\left(1 - \left(i\frac{Z_s}{\Phi}\frac{\alpha}{k_0}\right)^2\right)\tanh(\alpha A_c) + 2\frac{iZ_s}{\Phi}\frac{\alpha}{k_0} = 0. \tag{1}$$

A low frequency limit of Eq. (1) can be found when $\alpha A_c \ll 1$ and the dissipative effects are neglected. The solution of Eq. (1) is then approximated by

$$k_c = \beta k_0 = \sqrt{1 + \frac{2\Phi L_s}{A_c}}\,k_0. \tag{2}$$

The effective sound speed in the central tube is reduced by a factor $\beta \sim 5$. Thus, the TSSM will be efficient at a frequency 5 times smaller than a quarter wavelength resonator. When the frequency increases, Eq. (1) is solved numerically to find k_c and the effective sound speed in the central tube decrease from $c_0/5$ to 0 when a quarter wavelength resonance occurs in the side tubes. The entrance impedance of this continuous model is computed by $Z_c = -ik_0\cot(k_c L_c)/k_c$ and is plotted as a dotted blue line in Fig. 3.

The second model is a lumped model (Pierce, 1994). It assumes that the wave propagates in the central tube with lossy hard walls apart from the central position of the side branches where the pressure is continuous but a part of the acoustic velocity enters in the side branches. In the rigid parts, the impedance is transported through the relation

$$Z(x_2) = \frac{Z(x_1) + i\tan\left(k_r(x_2 - x_1)\right)}{1 + iZ(x_1)\tan\left(k_r(x_2 - x_1)\right)}, \tag{3}$$

valid for any position x_1 and x_2 along the tube, k_r is the wavenumber in the central tube accounting for the thermo-viscous losses. At the central position of the side branches, the impedance just before the discontinuity (Z^-) is linked to the impedance just after (Z^+) by

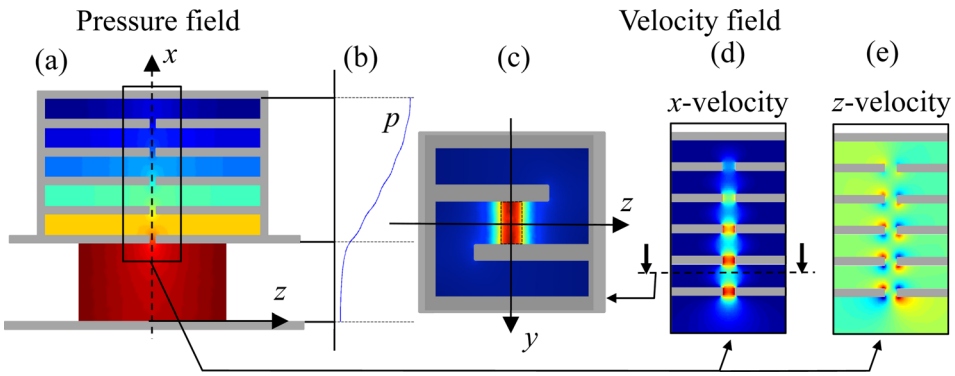

Fig. 4. (Color online) FEM simulation in a perfect fluid at 800 Hz. (a) Pressure field where the side branches has been unfolded, (b) shape of the pressure along the central line, (c) x-velocity in an y-z plane, (d) x-velocity in an x-z plane, and (e) z-velocity in an x-z plane.

$$Z^- = \left((Z^+)^{-1} + \frac{2S_s}{S_c} Z_s^{-1} \right)^{-1}, \tag{4}$$

where S_s and S_c are the areas of the side and central tubes. Then, starting from the rigid end of the central tube where the impedance is $Z(L_c) = \infty$ and applying alternatively Eqs. (3) and (4), the entrance impedance $Z_c = Z(x = 0)$ can be found. The advantage of this method is that the complex shape of the velocity field due to the geometry complexity (see Fig. 4) can be accounted for by means of added masses (Dubos *et al.*, 1999). In Eq. (4), we replace Z^+ with $Z^+ + \mathrm{i}k_0 l_1^{\mathrm{cor}}$, Z^- with $Z^- - \mathrm{i}k_0 l_1^{\mathrm{cor}}$ and Z_s with $Z_s + \mathrm{i}k_0 l_2^{\mathrm{cor}}$, where l_1^{cor} and l_2^{cor} are the correction lengths. Taking empirically $l_1^{\mathrm{cor}} = 0.6\,\mathrm{mm}$ and $l_2^{\mathrm{cor}} = 1.6\,\mathrm{mm}$, the result of the lumped model is plotted as a dashed red line in Fig. 3 and is in very good agreement with the measured impedance.

3. Use of TSSM in a duct with flow

The 4×8 cells TSSM ($D = 200\,\mathrm{mm} \times C = 100\,\mathrm{mm} \times L_c = 27\,\mathrm{mm}$) was mounted in the wall of a rigid rectangular duct as indicated in Fig. 1(b). The size of the duct is $C = 100\,\mathrm{mm} \times H = 15\,\mathrm{mm}$. Four microphones were flush mounted upstream and downstream of the TSSM. This allowed an over-determination of the incoming and outgoing waves on both sides of the TSSM. Two acoustic sources on both sides of the system gave two different acoustic states of the system and the four elements of the scattering matrix (transmission and reflection coefficient on both directions) for plane waves were evaluated. A more detail description of the measurement technic can be found in Aurégan and Leroux (2008). The measured transmission coefficients are plotted in Fig. 5 in the no-flow case and in the case of a grazing flow with a mean Mach number equal to $M = 0.2$.

Without flow, there is a large attenuation for three frequencies (654, 1710, and 2250 Hz). For the first peak (654 Hz), the transmitted pressure is reduced by 1000 (60 dB attenuation). This reduction is partly due to the attenuation in the material and partly due to the wave reflection on the TSSM. With flow, the attenuation is greatly reduced but occurs over a wider band. When the direction of wave propagation is opposite to the flow ($|T^-| \simeq 0.2$ at 700 Hz), the attenuation is greater than when the wave propagation and flow are in the same direction ($|T^+| \simeq 0.4$ at 700 Hz). Mitigation vanishes in the forbidden band of TSSM ($f > 2700\,\mathrm{Hz}$) without flow while a small but non-zero attenuation exists over the entire measured frequency range with flow.

To better understand this behavior, the convected Helmholtz equation is solved using a rigid boundary on the lower wall ($x = 0$). On the upper wall, the boundary is rigid outside of the TSSM and the Ingard-Myers boundary condition (IMBC): $(k_0 - Mk)^2 p = k_0 Z_{\mathrm{wall}}\, \partial_x p$ is applied on the material to account for the flow effects (Myers, 1980). To solve this problem, the convected Helmholtz equation is projected on the modes of the rigid duct accounting for the IMBC in the TSSM region. The scattering coefficients are found by matching this projection to the propagation of the plane wave in the rigid ducts on both sides of the material (Renou and Aurégan, 2011). The key parameter is the wall equivalent impedance that can be deduced from the entrance impedance Z_c of TSSM by $Z_{\mathrm{wall}} = (Z_c + Z_a)/\sigma$ where σ is the percentage of open area (POA) that is computed by dividing the section of the central tube by the

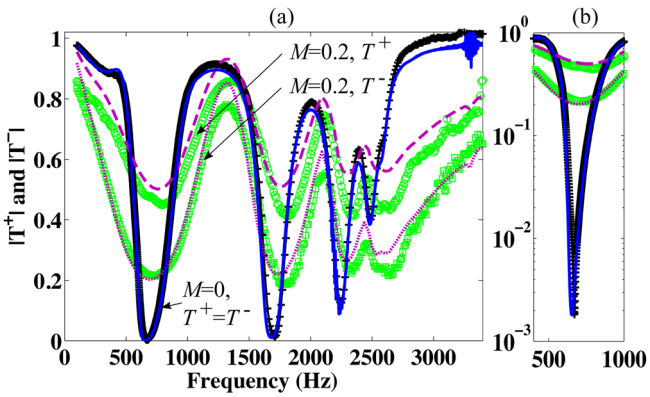

Fig. 5. (Color online) Modulus of the TSSM transmission coefficients. (a) The symbols represent the measured values (+: without flow, green circles: $M = 0.2$, in the flow direction T^+, green squares: $M = 0.2$, against the flow T^-). The lines represents the multimodal model results (blue continuous: without flow, magenta dashed: $M = 0.2$, T^+, magenta dotted: $M = 0.2$, T^-). (b) Zoom around the first peak in logarithmic scale.

section of the cell ($\sigma = A_c B_c / P^2 = 0.023$). Without flow, the added impedance Z_a accounts for the inertial effects in the main duct around the entrance of the TSSM, see Figs. 4(d) and 4(e), and is equal to $Z_a = ik_0 l_a$ where empirical added length is $l_a = 1.4$ mm. With flow, this added length is significantly reduced and a resistance linked to flow-acoustic interactions in the holes is added (Guess, 1975) which leads to $Z_a = R_a + ik_0 l_a$ with $R_a = 0.12$ and $l_a = 0.5$ mm (empirically determined). The results of this multimodal model are plotted as lines in Fig. 5 and confirm that this continuous model is suitable to represent the behavior of this TSSM composed of discrete cells because the frequency is much smaller than the Bragg frequency of the periodical system.

To find out if the resulting solution is optimal, the impedance Z_{wall} is compared to the Cremer optimal impedance. For the first attenuation peak (654 Hz) the resistance of the Cremer optimum ($R_{\text{Crem}} = 0.052$) for our channel height is much smaller that the TSSM resistance ($R_{\text{wall}} = 0.49$). This is mainly due to the very small value of the POA that divides the entrance resistance of the TSSM ($R_c = 0.011$) resulting from the thermal and viscous dissipations. The situation gets worse when the flow adds a resistance at the inlet holes of the TSSM and takes it away from the Cremer optimum value of resistance with flow which is approximately equal to $R_{\text{Crem}}/(1+M)^2$ (Tester, 1973b). In real applications, where the channel height is greater than that of our thin test duct, the optimal resistance is higher and more easily reachable. Therefore, for practical use of TSSM, a balance must be reached between the thickness reduction related to the parameter β and the POA for which an excessively low value results in a very high sensitivity to dissipation, to effects of grazing flow, and to large amplitude-related effects.

4. Conclusions

The TSSM, built around the recent concept of slow sound, shows its ability to strongly reduce transmitted sounds, especially at low frequencies, in airflow channels. A lumped discrete approach inside the TSSM allows an accurate modeling of the characteristics of this material. This material proves to be a possible solution for airflow channels when space constraints and dominant low frequency noise make the quarter-wavelength silencers unusable.

Acknowledgments

Y.A. and M.F. gratefully acknowledge the support from the European Union through ITN-project FlowAirS (Contract No. FP7-PEOPLE-2011-ITN-289352). J.-P.G. gratefully acknowledges the support from the ANR and FRAE through the project Metaudible (No. ANR-13-BS09-0003).

References and links

Aurégan, Y., and Leroux, M. (**2008**). "Experimental evidence of an instability over an impedance wall in a duct with flow," J. Sound Vib. **317**(3), 432–439.

Aurégan, Y., and Pagneux, V. (**2015**). "Slow sound in lined flow ducts," J. Acoust. Soc. Am. **138**(2), 605–613.

Dubos, V., Kergomard, J., Khettabi, A., Dalmont, J.-P., Keefe, D., and Nederveen, C. (**1999**). "Theory of sound propagation in a duct with a branched tube using modal decomposition," Acta Acust. Acust. **85**(2), 153–169.

Groby, J.-P., Huang, W., Lardeau, A., and Aurégan, Y. (**2015**). "The use of slow waves to design simple sound absorbing materials," J. Appl. Phys. **117**(12), 124903.

Guess, A. (**1975**). "Calculation of perforated plate liner parameters from specified acoustic resistance and reactance," J. Sound Vib. **40**(1), 119–137.

Le Roux, J. C., Pachebat, M., and Dalmont, J. P. (**2012**). "A new impedance sensor for industrial applications," in *Proceedings of the Acoustics 2012 Nantes Conference*, Nantes (April 23–27).

Li, D., Chang, D., and Liu B. (**2016**). "Enhancing the low frequency sound absorption of a perforated panel by parallel-arranged extended tubes," Appl. Acoust. **102**, 126–132.

Myers, M. (**1980**). "On the acoustic boundary condition in the presence of flow," J. Sound Vib. **71**(3), 429–434.

Pierce, A. D. (**1994**). Acoustics: An Introduction to its Physical Principles and Applications (Acoustical Society of America, Woodbury, NY), 678 pp.

Renou, Y., and Aurégan, Y. (**2011**). "Failure of the Ingard-Myers boundary condition for a lined duct: An experimental investigation," J. Acoust. Soc. Am. **130**(1), 52–60.

Tester, B. J. (**1973a**). "The optimization of modal sound attenuation in ducts, in the absence of mean flow," J. Sound Vib. **27**(4), 477–513.

Tester, B. J. (**1973b**). "The propagation and attenuation of sound in lined ducts containing uniform or 'plug' flow," J. Sound Vib. **28**(2), 151–203.

Tijdeman, H. (**1975**). "On the propagation of sound waves in cylindrical tubes," J. Sound Vib. **39**(1), 1–33.